

Nanoscale characterization of natural fibers and their composites using contact-resonance force microscopy [☆]

Sandeep S. Nair ^a, Siqun Wang ^{a,*}, Donna C. Hurley ^b

^a Tennessee Forest Products Center, University of Tennessee, Knoxville, TN, USA

^b Materials Reliability Division, National Institute of Standards & Technology, Boulder, CO, USA

ARTICLE INFO

Article history:

Received 6 July 2009

Received in revised form 5 January 2010

Accepted 16 January 2010

Keywords:

A. Polymer-matrix composites (PMCs)

A. Fibers

B. Interphase

B. Mechanical properties

ABSTRACT

Contact-resonance force microscopy (CR-FM) has been used for the first time to evaluate the mechanical properties of the interphase in natural fiber-reinforced composites and of cell wall layers of natural fibers. With CR-FM, quantitative images of the spatial distribution in nanoscale elastic properties were acquired. The images were calibrated with nanoindentation values. From the modulus images, the average interphase width was found to be (49 ± 5) nm for composite without any treatment, and (139 ± 21) nm for one with a maleic anhydride polypropylene treatment. There was a gradient of modulus across the interphase that ranged between the values of fiber and the polymer. The average values of indentation modulus obtained for different cell wall layers within a fiber were 22.5–28.0 GPa, 17.9–20.2 GPa, and 15.0–15.5 GPa for the S_2 and S_1 layers and the compound middle lamellae, respectively.

© 2010 Elsevier Ltd. All rights reserved.

1. Introduction

Natural fiber-reinforced polymer composites (NFRPCs) represent one of today's fastest growing industries. Possessing mechanical properties comparable to those of manmade fibers such as carbon, glass or aramid, natural fibers are a potential alternative in reinforced composites because of growing environmental awareness and legislated requirements. Natural fibers also have various advantages compared to conventional reinforcing fibers like glass and carbon fibers such as low cost, low density for an acceptable specific strength, low energy consumption, high toughness, high sound attenuation, nonabrasiveness, undergo little damage during processing, high degree of flexibility, less dermal and respiratory irritation, relatively reactive surface, ease of separation, renewable nature and biodegradability [1–8]. The combination of all these factors has prompted a number of industrial sectors, especially the automotive industry, to consider natural fibers as a substitute for conventional fibers in various products [9].

The interphase region between the reinforcing fiber and the bulk polymer matrix plays an important role in the performance of fiber-reinforced polymer composites. The structural integrity of a composite mainly depends on the quality of stress transfer in the interphase. The interphase formation depends on the property of components in use and modifications made on the compo-

nents [10]. Extending over lengths from nanometers to micrometers, a “well engineered” interphase is critical for desirable mechanical properties of fiber-reinforced polymer composites [9]. An interphase which has lower modulus than the surrounding polymer results in low composite stiffness and strength, but greater resistance to fracture [10,11]. On the other hand, an interphase with higher modulus than the surrounding polymer results in lower fracture resistance but greater strength [12]. While conventional fibers can be produced with a definite range of properties, the efficiency of natural fibers as reinforcements in composites depends on inherent factors such as structure, degree of crystallinity, polymerization, and orientation of cellulose chains. The major disadvantage of NFRPCs is the incompatibility between the hydrophilic natural fiber and the hydrophobic polymer, which can be improved only by either physical or chemical modification of the fiber or polymer [2,13]. Although various researchers have studied the effect of interphase on the bulk properties of composites [2,8,13], very little research has been done to characterize and provide quantitative measurements in the interphase. Previous NFRPC research on interphase characterization has consisted mostly of examining the fracture surfaces of broken composite samples with scanning electron microscopy (SEM). Because these studies examined the interaction between the fibers and the matrix based on the nature of fracture surface, the results only gave an indirect inference of interphase [14,15]. Nanoindentation and nanoscratching have also been used to quantify interphase mechanical properties on micrometer or submicrometer length scales. Lee et al. [16] evaluated the interphase properties of a natural fiber-reinforced polypropylene composite by nanoindentation and finite

Partial contribution of the National Institute of Standards and Technology; not subject to copyright in the United States.

* Corresponding author. Tel.: +1 865 9461120; fax: +1 865 9461109.

E-mail address: swang@utk.edu (S. Wang).

element analysis. Although they could not measure the interphase directly, their results indicated that the interphase width was less than 1 μm . More recently, researchers have used scanning probe microscopy (SPM) methods to get qualitative images and evaluate the extent of the interphase in various composites. Lee et al. [17] investigated the interfacial zone of a lyocell/polypropylene composite modified by maleated polypropylene (MAPP) using atomic force microscopy phase imaging (AFM-PI). Phase imaging records the phase lag when the AFM tip interacts with areas of different mechanical properties. They showed that the interphase transition zone ranged from approximately 113 nm to 128 nm. Since the measurements involving SPM involves complex geometric considerations, it has proved very difficult to obtain quantitative data on areas of different mechanical properties [18].

In addition to characterization of the composite interphase, a better understanding of the mechanical properties (modulus, hardness, yield stress and strength) of different fiber layers is necessary to improve the utilization of natural fibers as reinforcements in composites. Each wood fiber consists of different layers, as shown in Fig. 1. The primary wall of the fiber is the outermost layer, which is bound to the middle lamellae, which acts as a cementing agent between fibers. The primary cell walls of adjoining fibers, together with the middle lamellae in between, form the compound middle lamellae (CML). The secondary wall is divided into the S_1 , S_2 and S_3 layers. The orientation of the cellulose microfibrils within each cell wall layer strongly influences the mechanical properties of natural fibers in their longitudinal direction [19]. The orientation of the cellulose microfibrils is nearly perpendicular (flat helix) to the fiber axis in the S_1 and S_3 layers, while it is almost parallel (steep helix) to the fiber axis in the S_2 layer [20,21]. Using theoretical cell wall unit models, Watanabe and Norimoto [22] showed that the longitudinal modulus of the S_2 layer decreased as the microfibril angle with respect to the fiber axis increased. Several researchers have studied the mechanical properties of single wood fibers, mainly with nanoindentation, atomic force microscopy (AFM), or a combination of both. However, most of these studies were conducted on refined natural fibers [23] or isolated single cellulose fibrils [24], both of which are prone to mechanical or chemical modification. Nanoindentation is currently one of the most-used methods to quantify the mechanical properties of cell wall layers of natural fibers. Due to the limits of its spatial resolution, most nanoindentation studies have been confined to the S_2 layer. These studies have considered annual rings [25], lignifications [26], comparisons with middle lamellae, melamine modified wood [27], and early or late wood [28]. Wimmer and Lucas [29] conducted nanoindentation on the S_2 layer and CML and obtained an average value of 16 GPa for the longitudinal modulus of the S_2 layer, double the value for the CML. Their indentation test on the CML was confined to the cell corner middle lamellae due to the narrowness of the CML layer. Since the average thickness of the S_1 layer is approximately 0.4 μm and that of the CML layer is

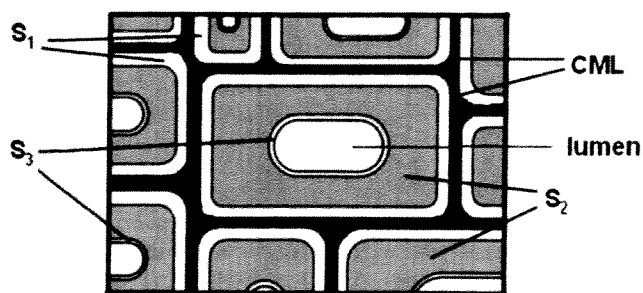


Fig. 1. Schematic representation of cell wall layers.

around 0.1 μm , the mechanical properties of these layers have rarely been studied. Zhang et al. [30] investigated the strength and fracture behavior of wood cell wall S_2 layer through an uniaxial micro-compression test and obtained the value of 125 MPa for the compression strength for loblolly pine. Attempts to characterize fiber layers such as S_1 and S_3 with various microscopic methods have yielded only qualitative results [31,32].

The above discussion highlights the need for a measurement method capable of providing quantitative information about mechanical properties with nanoscale spatial resolution, while at the same time providing images of the spatial distribution in properties. Such a method would prove invaluable for studies of the interphase region in NFRPCs as well as of cell wall layers. Here we show how contact-resonance force microscopy (CR-FM) methods [33] can be used to meet this need. CR-FM has the imaging capability of AFM, combined with the ability to determine quantitative modulus values. In this way, it is possible to image or visualize the nanoscale spatial distribution of properties, rather than relying on a single average value or a point by point estimation of quantitative values.

2. Materials and methods

2.1. Materials and sample preparation¹

For the NFRPC experiments, isotactic polypropylene (PP) (Exxon Mobil Corporation, Irving, TX) with a melt flow index of 35 and maleated polypropylene (MAPP) (Epolene G-3003, Eastman Chemicals, Kingsport, TN) were used. Dry solid states of PP and MAPP were mixed with a HAAGA MiniLab extruder (Thermo Fischer Scientific, Karlsruhe, Germany). The temperature, rotation speed, and processing period were 180 $^{\circ}\text{C}$, 100 rpm, and 10 min, respectively. One mixture contained 10 wt.% of MAPP, while the other contained 0% MAPP. The dry mixtures were compression molded into films approximately 0.25 mm thick. Lyocell fibers (Lenzing AG, Lenzing, Austria) approximately 10 μm in diameter and 30 μm long were unidirectionally placed on top of the PP-MAPP films. The films were then stacked and compression molded at 200 $^{\circ}\text{C}$ for 10 min in order to obtain unidirectional lyocell fiber-reinforced composites [34]. The cell wall layer experiments involved samples collected from a 45-year-old red oak. A latewood portion of the 45th annual ring was cut with dimensions of 2 mm \times 5 mm \times 5 mm in the radial, tangential and longitudinal directions, respectively.

The NFRPC and cell wall samples were embedded in an epoxy medium under vacuum and cured by heating and drying for 8 h at 70 $^{\circ}\text{C}$ [35]. A cross section of the sample was prepared by use of an ultramicrotome with a diamond knife. The microtome process yielded sufficiently smooth surfaces for the CR-FM experiments.

2.2. Nanoindentation techniques

Modulus values for the lyocell fiber and PP matrix for the composites and the S_2 layer of the wood sample were obtained by displacement-controlled nanoindentation (Triboindenter, Hysitron, Eden Prairie, MN). The Berkovich indenter tip was loaded to a maximum displacement of 250 nm. The indentation modulus of the sample is inferred from the initial unloading contact stiffness S , i.e., the slope dP/dh of the tangent to the initial unloading curve

¹ Commercial equipment, instruments, or materials are identified only in order to adequately specify certain procedures. In no case does such identification imply recommendation or endorsement by the National Institute of Standards and Technology, nor does it imply that the products identified are necessarily the best available for the purpose.

in the load–displacement curve, where P is the indentation force and h is the displacement. The sample reduced indentation modulus (E_r) is then calculated from [36]

$$E_r = \frac{\sqrt{\pi}}{2\beta} \frac{S}{\sqrt{A}} \quad (1)$$

where β is a constant that depends on the geometry of the indenter ($\beta = 1.034$ for a Berkovich indenter) and A is the contact area. The indentation modulus M_s of the sample is then obtained from

$$\frac{1}{E_r} = \frac{1}{M_s} + \frac{1}{M_{tip}} \quad (2)$$

where M_{tip} is the indentation modulus of the diamond indenter tip. The value $M_{tip} = 1146$ GPa was used [37]. The average value of M for the S_2 layer obtained by nanoindentation was 24.6 GPa. The average indentation modulus reference values for the composites obtained by nanoindentation on the fiber and matrix were $M_{fiber} = 12.4 \pm 0.3$ GPa and $M_{matrix} = 3.2 \pm 0.3$ GPa, respectively.

2.3. CR-FM techniques

Contact-resonance force microscopy (CR-FM) [33] was used for quantitative imaging of the nanoscale elastic properties of the samples. CR-FM is based on the atomic force acoustic microscopy (AFAM) method [38,39], which determines elastic properties at a fixed sample position. The basic measurement procedure involves measuring the resonant frequencies of the vibrating AFM cantilever in both free space and when the tip is in contact with the sample. From the measured resonant frequencies, values are determined for the contact stiffness k^* describing the elastic interaction between the tip and the sample. The indentation modulus is then determined from the contact stiffness with a model for the tip-sample contact mechanics [33,38,39].

An extension of AFAM for quantitative imaging, CR-FM techniques have been described in detail elsewhere [33,40,41]. The imaging experiments were performed with custom electronics that

interface with a commercial AFM instrument [42]. A conceptual schematic of the experimental apparatus is shown in Fig. 2. The sample under investigation is bonded to a piezoelectric actuator (ultrasonic transducer) affixed to the positioning stage of the AFM instrument. The transducer is driven by a swept sine wave voltage, and the resulting vibrations excite the resonant modes of the cantilever. The signal from the AFM position-sensitive photodiode is used as input to the custom electronics in order to determine the contact resonance frequency at a given image position. Through the use of an auxiliary AFM input channel, an image of these frequencies is acquired in parallel with the topographic image.

The AFM cantilevers used in these experiments had nominal dimensions of length $L = 225 \pm 10 \mu\text{m}$, width $w = 30 \pm 8 \mu\text{m}$, and thickness $t = 3 \pm 1 \mu\text{m}$, and nominal spring constant $k_c = 2.8$ N/m. The applied static force $F_N = k_c d$, where d is the deflection, was approximately 50–80 nN. To avoid registration difficulties and artifacts due to scanner drift and hysteresis in scanning the same area twice, frequency images were acquired for only one resonant mode, namely the second flexural mode [41]. The second mode is the most sensitive mode for the experimental conditions used here, that is, it exhibits the greatest change in resonant frequency for a given change in contact stiffness [33].

Images of the normalized contact stiffness k^*/k_c for a sample (“test”) region were calculated from the frequency images assuming a fixed value for the relative tip position $L_1/L = 0.97$, where L_1 is the position of tip relative to the total length L of the cantilever. This approach was feasible due to the relatively small variation in contact stiffness with L_1/L for the second flexural mode [33]. The contact stiffness images were transformed into images of the reduced modulus E_{test}^* by use of the nanoindentation measurements on a reference specimen. It is necessary to convert the reduced modulus value E_r obtained by nanoindentation with a diamond tip into a reduced modulus E_{ref}^* corresponding to contact with the AFM tip. A relation identical to Eq. (2) is used, except that $M_{tip} = 165$ GPa for the (001) silicon tip. Values of the reduced

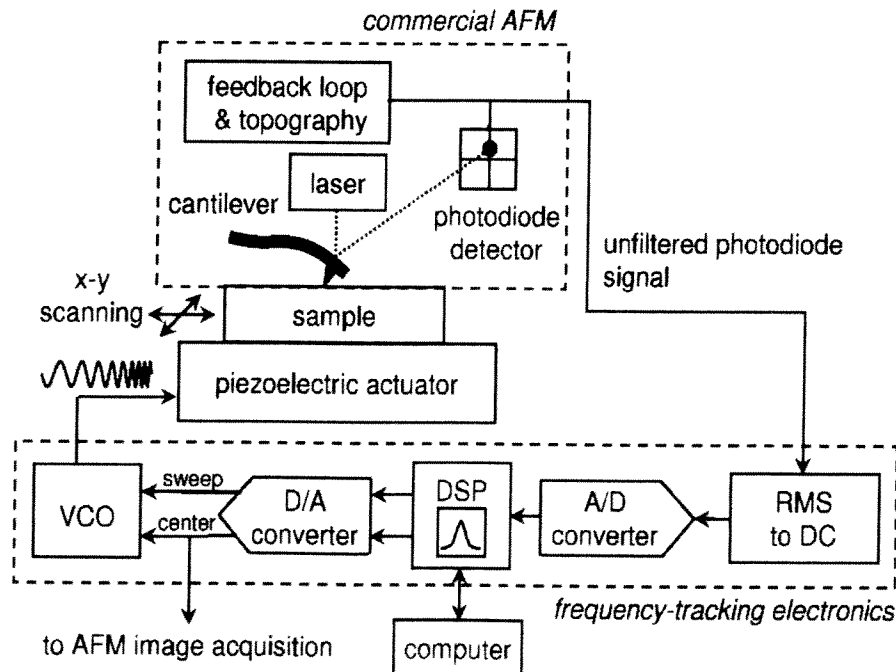


Fig. 2. Schematic representation of CR-FM apparatus for modulus mapping. From right to left, the custom electronics comprise a root-mean-square (RMS) to direct current (DC) converter, analog-to-digital (A/D) converter, a digital signal processor (DSP), a digital to analog (D/A) converter, and a voltage-controlled oscillator (VCO) to drive the piezoelectric actuator.

modulus E_{test}^* for the sample region were then calculated with [33,38,39]

$$E_{test}^* = E_{ref}^* \left(\frac{k_{test}^*}{k_{ref}^*} \right)^n \quad (3)$$

where k_{test}^* and k_{ref}^* are the contact stiffness values for the test sample and reference sample, respectively. The value $n = 3/2$ was used, corresponding to Hertzian contact. Finally, the reduced modulus images were converted to images of the indentation modulus M_{test} using Eq. (2).

This approach was used to calculate indentation modulus values for the images of the cell wall layers. E_r and hence M_{ref} and E_{ref}^* were obtained by nanoindentation for the S_2 layer. For each experimental image, the mean value of the contact stiffness was determined for a region containing the S_2 layer and was used as k_{ref}^* in Eq. (3). For images of the composite interphase, a dual reference approach was used. Nanoindentation values for both the fiber (M_{fiber}) and the matrix (M_{matrix}) were obtained and used in [43]

$$M_{test} = \frac{\left(\frac{k_{fiber}^*}{k_{matrix}^*} \right)^n - 1}{\left(\frac{k_{fiber}^*}{k_{test}^*} \right)^n \left(\frac{1}{M_{matrix}} - \frac{1}{M_{fiber}} \right) + \left(\frac{k_{fiber}^*}{k_{matrix}^*} \right)^n \left(\frac{1}{M_{fiber}} - \frac{1}{M_{matrix}} \right)} \quad (4)$$

in this case, two reference values of the contact stiffness were determined for each image. One value was the average value k_{fiber}^* for an image region that contained only the fiber, and one was the average value k_{matrix}^* for a region that contained only the matrix.

3. Results and discussion

3.1. Evaluation of interphase in fiber-reinforced composites

Contact resonance frequency images were obtained at the boundary region between the fiber and the matrix. In order to avoid signal artifacts due to topographical effects, regions as flat as possible were selected (height ~ 20 nm or less) for imaging. Fig. 3 shows indentation modulus images for two composite samples with different treatments. Differences in modulus values for the fiber, fiber–matrix boundary zone, and matrix regions are clearly visible in the images. The interphase zone properties were analyzed with commercial image processing software. Mean indentation modulus values for regions consisting entirely of fiber and matrix were obtained from the area enclosed within the box plots shown in Fig. 4a. Fig. 4b shows the line profile corresponding to the radial line segment in Fig. 4a across the fiber–matrix boundary region. The left pointer in Fig. 4b corresponds to the mean indentation value for the fiber (12.4 GPa), while the right pointer indicates that of the matrix (3.2 GPa). In Fig. 4b, the distance between the two pointers, where the properties differ from those of the bulk fiber and matrix corresponds to the interphase thickness (in this case was about 135 nm). By definition, the interphase starts from some point on the fiber where the local properties, as a result of various surface treatments or reaction with the matrix, begin to change from those of the bulk fiber and extends until the local properties equal the bulk matrix properties [10]. In order to minimize any morphological variations near the fiber or the matrix surface, this approach was applied to 15 radial lines across the fiber–matrix boundary. The width of interphase obtained by averaging these line scans was found to be (49 ± 5) nm for the composite without MAPP treatment, and (139 ± 21) nm for the one with 10% MAPP treatment. Fig. 5 shows the line profiles obtained by averaging 15 radial line scans across the fiber–matrix boundary region for both composites. The average line profile for each composite exhibited a gradient of modulus across the interphase region that ranged between the modulus values of fiber and the polymer.

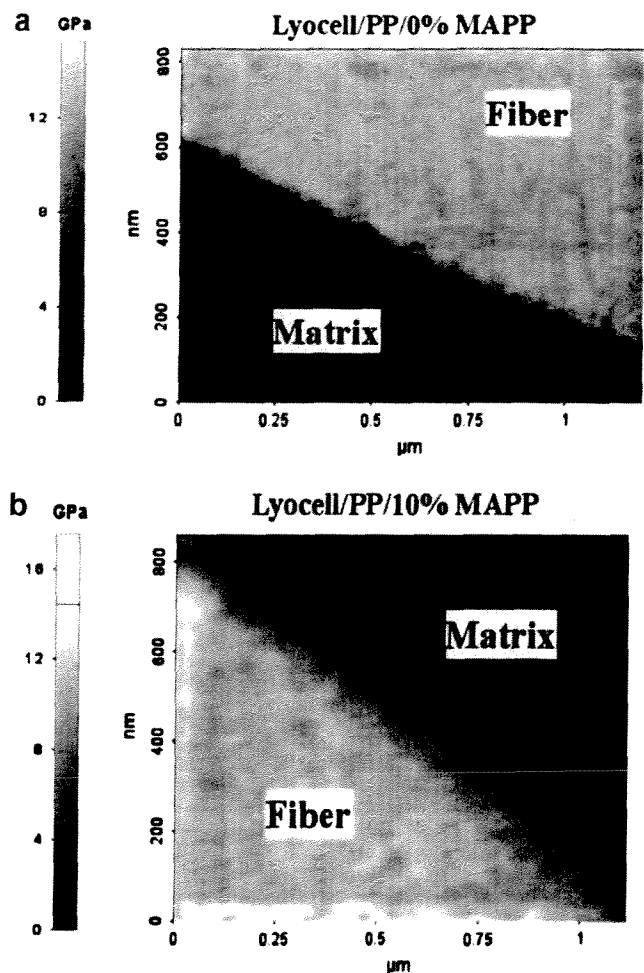


Fig. 3. Indentation modulus images for: (a) lyocell/PP composites without treatment and (b) with MAPP treatment.

As mentioned above, chemical modification of the hydrophilic fiber and/or the hydrophobic matrix is necessary for a strong fiber–matrix bond. These results indicate that the MAPP treatment has substantially increased the interphase transition zone. This is consistent with previous results in the literature. For instance, Lee et al. [17] showed that the use of MAPP as a compatibilizer in lyocell/polypropylene composite increased the interphase transition zone. Also, they have shown that the combined use of MAPP and γ -amino propyltrimethoxy silane (γ -APS) have further increased the interphase transition zone.

Interphase widths of less than 100 nm with quantitative mechanical measurements at each position have rarely been reported in the literature. The main reason for this is the lack of techniques that can measure the properties with such nanoscale spatial resolution. Griswold et al. [44] examined the interphase region of an epoxy/glass composite with AFM-PI and nanoindentation and showed that the interphase thickness varied between 110 nm and 888 nm for different silane concentrations. Although they used SPM methods such as AFM-PI that possess the spatial resolution needed to characterize such narrow interphases, the lack of ability to provide quantitative measurements at each position in the interphase was a major drawback. Hodzic et al. [45] conducted nanoindentation and nanoscratching on polymer/glass composite systems and reported that the interphase varied between 2 μ m and 6 μ m. Kim et al. [46] found that the interphase width measured by nanoscratching for a polymer/glass system varied from

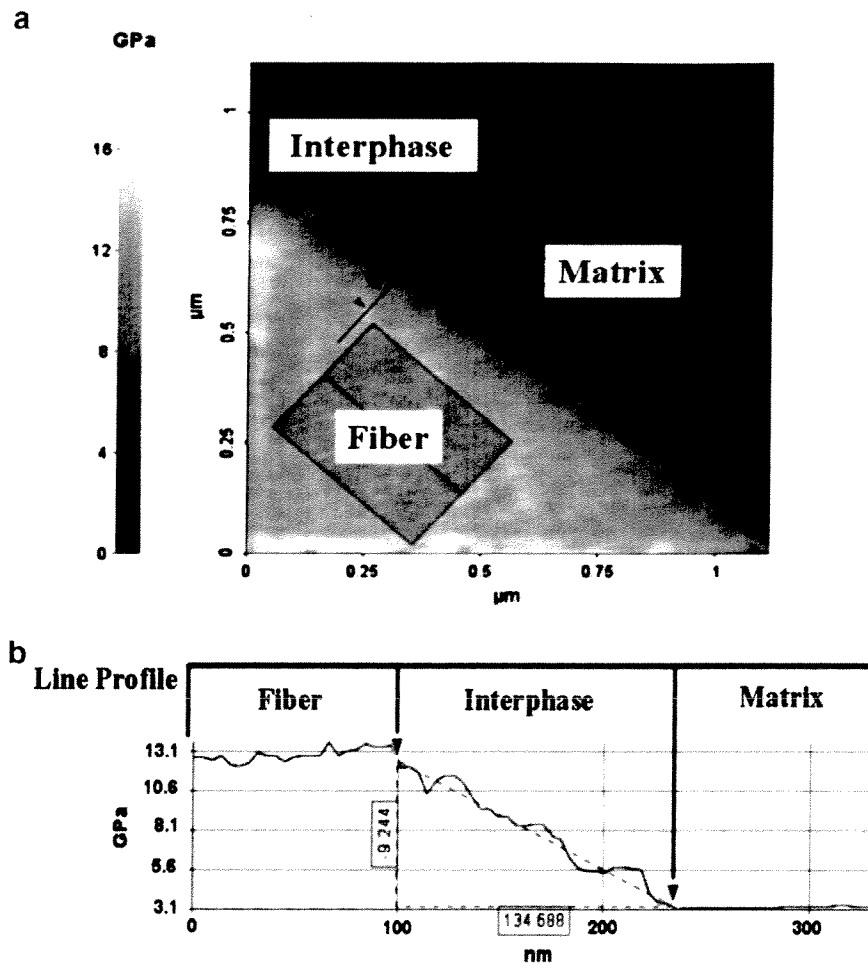


Fig. 4. (a) Analysis of the modulus, and (b) line profile image showing the size of interphase based on the gradient in modulus.

0.8 μm to 1.5 μm , and that the width increased with silane concentration.

All of these values are much larger than the values obtained in this study. One explanation is that the limited spatial resolution of nanoindentation prevents accurate measurements of narrow interphases. In addition to the limit imposed by the size of the indenter tip, the lateral resolution is reduced by other effects. The spacing of indents made by nanoindentation should be sufficiently wide enough to avoid the overlapping of the zone associated by plastic deformation. For instance, finite element analysis has shown that the interphase thickness measured by nanoindentation can appear larger than the true value due to the effect of neighboring materials [16]. In this study involving the CR-FM technique, we have demonstrated the ability to measure interphase zones as narrow as 50 nm in lyocell/polypropylene composites. The extremely small tip radius (25–35 nm) and low forces (50–80 nN) involved in these CR-FM experiments mean that the deformation of the sample surface is very small and is elastic. This feature is quite valuable for characterizing the narrow interphase widths in NFRPCs.

3.2. Evaluation of mechanical properties of cell wall layers

Contact resonance frequency images were obtained at the boundary region between two fibers within the growth ring. Modulus maps were calculated from the frequency images using the procedure described above. Fig. 6 shows images for the topography and indentation modulus. Contrasts in modulus between the CML and S_1 and S_2 layers are clearly visible. Mean values of the indenta-

tion modulus for the CML and S_1 and S_2 layers were obtained from the area enclosed within the box plots, as shown in Fig. 6. To avoid signal artifacts due to topographical effects, regions as flat as possible were selected for the box plot analysis. The values of indentation modulus were 22.5–28.0 GPa, 17.9–20.2 GPa, and 15.0–15.5 GPa for the S_2 , S_1 , and CML layers, respectively. The higher values of the S_2 layer compared to other layers are consistent with previous results in the literature [29,47]. Although the S_2 layer has a steeper helix and the S_1 layer has a flatter helix of microfibril orientation with respect to the fiber axis, various studies have shown that there is a shift of microfibril orientation from the outer S_1 layer to the inner S_2 layer and from the outer S_2 layer to the inner S_3 layer. Abe et al. [48] reported that the cellulose microfibril orientation in the secondary cell wall layers of Sakhalin fir, as seen from the lumen side, gradually changed in a clockwise direction from the outermost S_1 to the middle of the S_2 and then to counterclockwise to the innermost S_3 . Xing et al. [49] examined the cell wall layers of refined fibers of loblolly pine by use of nanoindentation and showed that there exists a clear interphase between S_2 and S_1 and between S_2 and S_3 . The wider range of indentation modulus values obtained in this study for each of the secondary layers can be explained partly by differences in the cellulose microfibril angle within each layer [19,22].

The images in Fig. 6 also show a thin region between the S_1 and S_2 layers with apparently lower modulus than that of other secondary layers. Line profile analysis of these regions, as shown in Fig. 7, indicates that signal artifacts due to topography are the most likely cause of the effect. In CR-FM experiments, the measured resonant

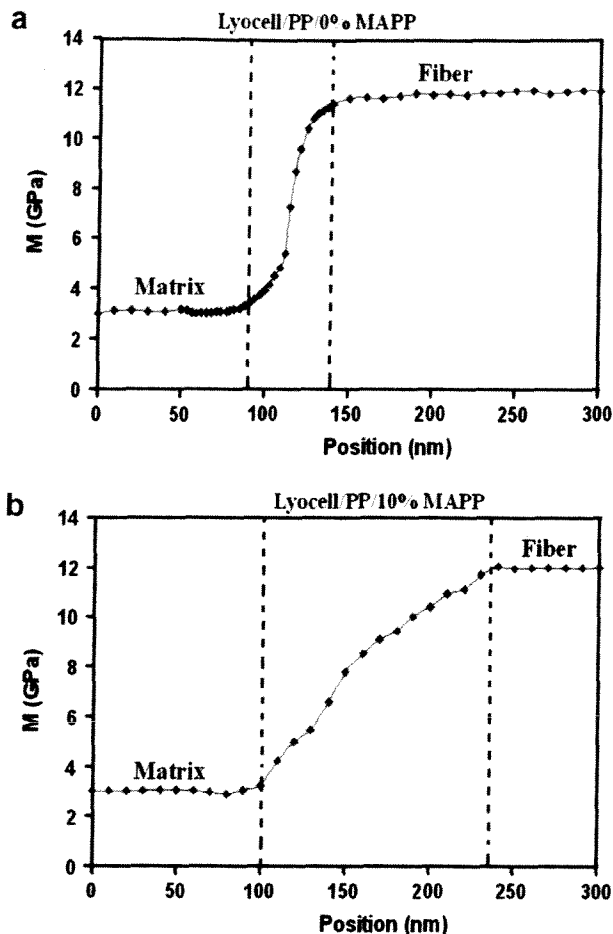


Fig. 5. Average modulus across interphase region (between the vertical dotted lines) between the fiber and matrix for: (a) lyocell/PP composites without any treatment and (b) with MAPP treatment.

frequency depends not only on the local contact stiffness, but also on the contact area between the tip and sample. For a perfectly flat sample, the contact area remains the same during scanning, and frequency changes correspond only to contact stiffness variations. However, as indicated in Fig. 8, sharp or significant changes in topography will affect the contact area. The resulting change in frequency leads to false changes in modulus. Finally, the innermost layer of the fiber, the S_3 layer, could not be reliably identified in the CR-FM modulus maps. Because it is adjacent to the lumen and is the thinnest layer, the distinction of this layer might have been lost when the lumen region was replaced with epoxy during sample preparation. Improved sample preparation methods are required in order to better characterize this layer with CR-FM techniques.

CR-FM methods present a number of advantages over other methods for studying the elastic properties of cell walls. Because it is the thickest cell wall layer, the S_2 layer has been the subject of earlier studies. The presence of various adjacent layers in fibers can alter the deformation fields surrounding indents made by nanoindentation, potentially leading to incorrect estimates of the indentation modulus. Jakes et al. [50] showed that the structural compliance observed in nanoindentation experiments on the S_2 layer was mainly due to the effect of the nearby free edge of the lumen. In CR-FM technique, the fact that the deformation is much smaller and elastic largely solves this problem. The improvement in lateral spatial resolution afforded by CR-FM methods using a smaller tip and lower applied forces opens the door to detailed studies of cell wall structure. CR-FM also provides an image of

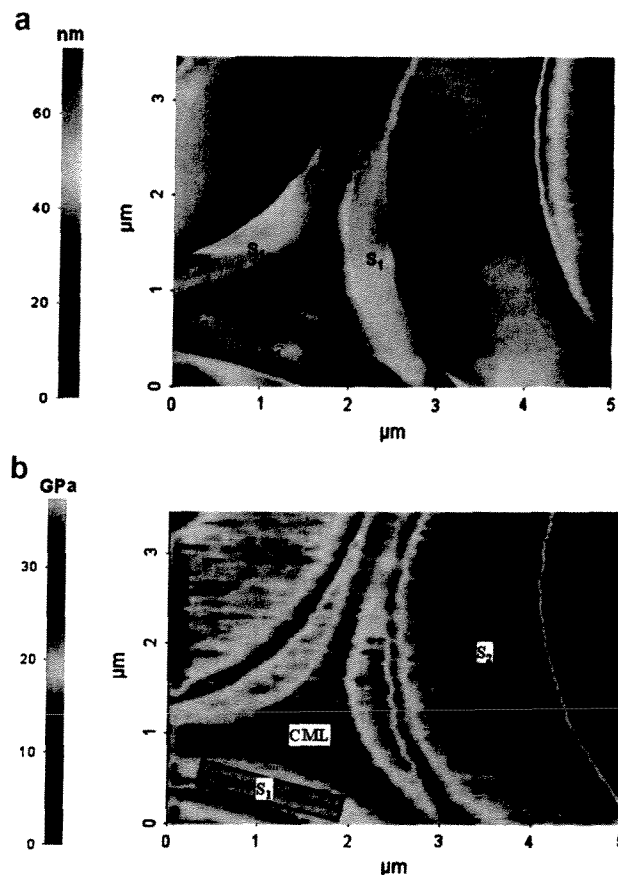


Fig. 6. Images of: (a) topography and (b) box plot analysis of indentation modulus image of various cell wall layers.

quantitative modulus values, in contrast to many other AFM methods. For instance, the AFM methods used by Clair et al. [47] to investigate holm oak and boco wood specimens provide only qualitative images of elastic contrast and quantitative values at only a handful of sample positions. The ability of contact-resonance methods to provide quantitative images of nanoscale mechanical properties has not been demonstrated in any of the previously conducted cell wall studies.

4. Conclusion

This study demonstrates that contact-resonance force microscopy is a valuable technique for evaluating the interphase of natural fiber-reinforced polymer composites and for characterizing the elastic properties of cell wall layers of natural fibers. The nanoscale spatial resolution of CR-FM, combined with its ability to provide quantitative modulus images, makes it possible to investigate the mechanical properties of interphases as narrow as 50 nm in NFRPCs and thin cell wall layers in natural fibers. This technique, which has previously been used to characterize various micro- and nano structures, is used here for the first time in the field of natural fibers. The extremely low loads and small tip radius characteristic of CR-FM enables *in situ* elastic property information with significantly higher spatial resolution than other, destructive methods like nanoindentation. The use of a reference material with similar modulus values removes much of the uncertainty arising in the final modulus values from tip wear and tear, which is very common with other AFM methods. These results suggest that this method will enable researchers to get much more information about the nanoscale properties of interphase and fibers, and

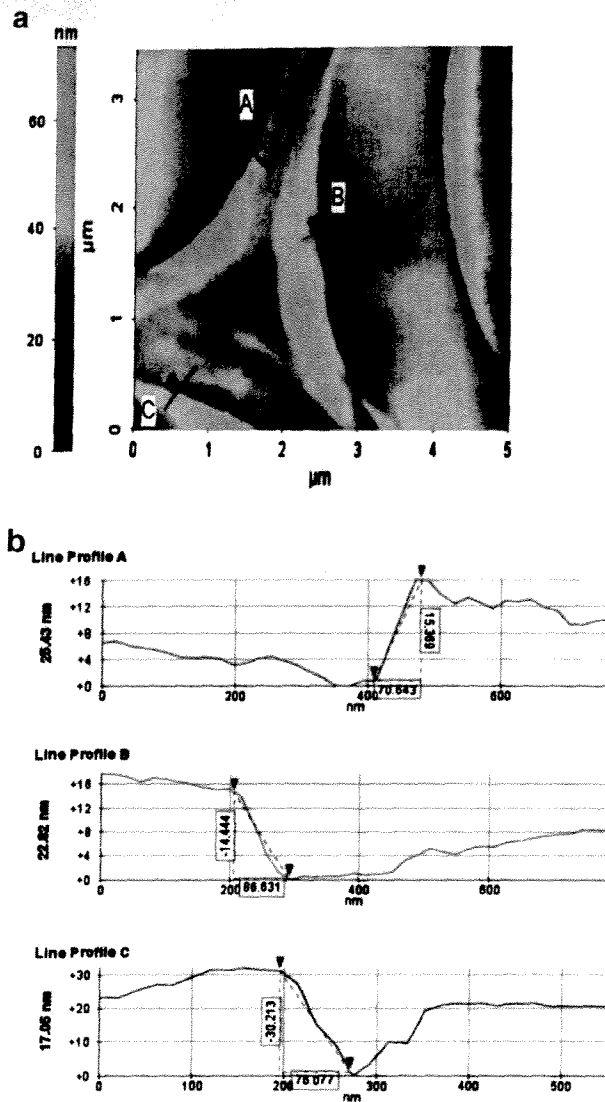


Fig. 7. (a) Topographical change between S_1 and S_2 and (b) corresponding line profile.

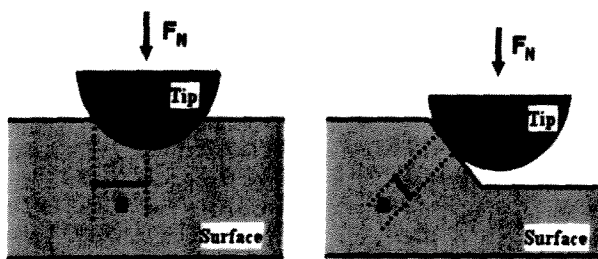


Fig. 8. (a) Schematics for contact mechanics for Hertzian contact on flat surface (left) and on a steep slope (right).

correlate these information to macroscale performance provides an interesting direction for future work, which is very important for optimum design of final NFRPC products.

Acknowledgements

The authors thank Dr. John Dunlap and Dr. Cheng Xing at the University of Tennessee for their kind help in preparing the sam-

ples with the microtome and helping with the nanoindentation measurements. The project was supported by the National Research Initiative of the USDA Cooperative State Research, Education, and Extension Service, Grant #2005-02645, the USDA Wood Utilization Research Grant and partly supported by the Natural Science Foundation of China #30928022.

References

- [1] Bledzki AK, Letman M, Viksne A, Rence L. A comparison of compounding processes and wood type for wood fibre-PP composites. *Compos Part A: Appl Sci Manuf* 2005;36(6):789–97.
- [2] Lee SH, Wang S. Biodegradable polymers/bamboo fiber biocomposite with bio-based coupling agent. *Compos Part A: Appl Sci Manuf* 2006;37(1):80–91.
- [3] Liao B, Huang Y, Cong G. Influence of modified wood fibers on the mechanical properties of wood fiber-reinforced polyethylene. *J Appl Polym Sci* 1997;66:1561–8.
- [4] Mathew L, Joseph R. Mechanical properties of short-isora-fiber-reinforced natural rubber composites: effects of fiber length, orientation, and loading, alkali treatment, and bonding agent. *J Appl Polym Sci* 2007;1640–50.
- [5] Franco P, Gonzalez JH. Mechanical properties of continuous natural fibre-reinforced polymer composites. *Compos Part A: Appl Sci Manuf* 2003;35:339–45.
- [6] Wollerdorfer M, Barder H. Influence of natural fibers on the mechanical properties of biodegradable polymers. *Ind Crops Prod* 1998;8:105–12.
- [7] Mohanty AK, Misra M, Hinrichsen G. Biofibers, biodegradable polymers and biocomposites: an overview. *Macromol Mater Eng* 2000;276/277:1–24.
- [8] Coutinha FMB, Costa THS, Carvalho DL. Polypropylene-wood fiber composites: effect of treatment and mixing conditions on mechanical properties. *J Appl Polym Sci* 1997;65:1227–35.
- [9] Mohanty AK, Misra M, Drzal LT. Surface modifications of natural fibers and performance of the resulting biocomposites: an overview. *Compos Interfaces* 2001;8(5):313–43.
- [10] Drzal LT. The interphase in epoxy composites. *Adv Polym Sci* 1986;75:1–32.
- [11] Williams JG, Donnellan ME, James MR, Morris WL. Properties of the interphase in organic matrix composites. *Mater Sci Eng A* 1990;126:305–12.
- [12] Drzal LT, Rich MJ, Koenig MF, Lloyd PF. Adhesion of graphite fibers to epoxy matrices. 2. The effect of fiber finish. *J Adhes* 1983;16(2):133–52.
- [13] Gassan J, Bledzki A. The influence of fiber-surface treatment on the mechanical properties of jute-polypropylene composites. *Compos Part A: Appl Sci Manuf* 1997;28A:1001–5.
- [14] Oksman K, Clemons C. Mechanical properties and morphology of impact modified polypropylene-wood flour composites. *J Appl Polym Sci* 1997;67:1503–13.
- [15] Felix JM, Gatenholm P. The nature of adhesion in composites of modified cellulose fibers and polypropylene. *J Appl Polym Sci* 1991;42:609–20.
- [16] Lee SH, Wang S, Pharr GM, Xu H. Evaluation of interphase in a cellulose fiber-reinforced polypropylene composite by nanoindentation and finite element analysis. *Compos Part A: Appl Sci Manuf* 2007;38:1517–24.
- [17] Lee SH, Wang S, Takashi E, Kim NH. Visualization of interfacial zones in lyocell fiber-reinforced polypropylene composite by AFM contrast imaging based on phase and thermal conductivity measurements. *Holzforschung* 2009;63:240–7.
- [18] Munz M, Sturm H, Schulz E, Hinrichsen G. The scanning force microscope as a tool for the detection of local mechanical properties within the interphase of fiber reinforced polymers. *Compos Part A* 1998;29:1251–9.
- [19] Bergander A, Salmen L. Cell wall properties and their effects on the mechanical properties of fibers. *J Mater Sci* 2002;37:151–6.
- [20] Brandstrom J. Micro- and ultrastructural aspects of Norway spruce tracheids: a review. *IAWA* 2001;22(4):333–53.
- [21] Donaldson L, Xu P. Microfibril orientation across the secondary cell wall of radiate pine tracheids. *Trees* 2005;19:644–53.
- [22] Watanabe U, Norimoto M. Three dimensional analysis of elastic constants of the wood cell wall. *Wood Research* 2000;87:1–7.
- [23] Xing C, Wang S, Pharr GM. Comparison of the effects of thermomechanical refining pressure on the properties of refined fibers of juvenile and mature wood. *Wood Sci Technol* 2009;43:615–25.
- [24] Cheng Q, Wang S. A method for testing the elastic modulus of single cellulose fibrils via atomic force microscopy. *Compos Part A: Appl Sci Manuf* 2008;39:1838–43.
- [25] Tze WTY, Wang S, Rials TG, Pharr GM, Kelley SS. Nanoindentation of wood cell walls: continuous stiffness and hardness measurements. *Compos Part A: Appl Sci Manuf* 2007;38:945–53.
- [26] Gindl W, Gupta HS, Grunwals C. Lignification of spruce tracheid secondary cell walls related to longitudinal hardness and modulus of elasticity using nano-indentation. *Can J Botany* 2002;80:1029–33.
- [27] Gindl W, Gupta HS. Cell-wall hardness and Young's modulus of melamine-modified spruce wood by nano-indentation. *Compos Part A: Appl Sci Manuf* 2002;33:1141–5.
- [28] Wimmer R, Lucas BN, Tsui TY, Oliver WC. Longitudinal hardness and Young's modulus of spruce tracheid secondary walls using nanoindentation. *Wood Sci Technol* 1997;31:131–41.
- [29] Wimmer R, Lucas BN. Comparing mechanical properties of secondary wall and cell corner middle lamellae in spruce wood. *IAWA* 1997;18(1):77–88.

- [30] Zhang X, Zhao Q, Wang S, Trejo R, Lara-Curzio E, Du G. Characterizing strength and fracture of wood cell wall through uniaxial micro-compression test. *Compos Part A: Appl Sci Manuf* 2010;41:632–8.
- [31] Fahlen J, Salmen L. Cross-sectional structure of the secondary wall of wood fibers as affected by processing. *J Mater Sci* 2003;38:119–26.
- [32] Fahlen J, Salmen L. On the lamellar structure of the tracheid wall. *Plant Biol* 2002;4:339–45.
- [33] Hurley DC. Contact resonance force microscopy techniques for nanomechanical measurements. In: Bhushan B, Fuchs H, editors. *Applied scanning probe methods*, vol. XI. Berlin: Springer-Verlag; 2009. p. 97–138.
- [34] Nair SS, Wang S, Hurley DC. Evaluation of interphase properties in fiber reinforced polymer composite using contact resonance force microscopy. In: *Proceedings of the 51st annual meeting of the society of wood science and technology (Concepción, Chile, 10–12 November 2008)*.
- [35] Spur AR. A low-viscosity epoxy resin embedding medium for electron microscope. *J Ultrastruct Res* 1969;26:31–43.
- [36] Oliver WC, Pharr GM. An improved technique for determining hardness and elastic modulus using load and displacement sensing indentation experiments. *J Mater Res* 1997;7(6):1564–83.
- [37] Kopycinska-Müller M, Geiss RH, Müller J, Hurley DC. Elastic property measurements of ultra thin films using atomic force acoustic microscopy. *Nanotechnology* 2005;16:703–9.
- [38] Rabe U, Amelio S, Kester E, Scherer V, Hirsekorn S, Arnold W. Quantitative determination of contact stiffness using atomic force acoustic microscopy. *Ultrasonics* 2000;38:430–7.
- [39] Hurley DC, Shen K, Jennett NM, Turner JA. Atomic force microscopy methods to determine thin film elastic properties. *J Appl Phys* 2003;94(4):2347–54.
- [40] Hurley DC, Kopycinska-Müller M, Kos AB. Mapping mechanical properties on the nanoscale with atomic force acoustic microscopy. *JOM* 2007;59: 23–9.
- [41] Hurley DC. Measuring mechanical properties on the nanoscale with contact resonance force microscopy methods: scanning probe microscopy of functional materials. In: Kalinin S, Gruverman A, editors. *Nanoscale imaging and spectroscopy*. Berlin: Springer-Verlag, in press.
- [42] Kos AB, Hurley DC. Nanomechanical mapping with resonance tracking scanned probe microscope. *Meas Sci Technol* 2008;19:015504.
- [43] Stan G, Price W. Quantitative measurements of indentation moduli by atomic force acoustic microscopy using a dual reference method. *Rev Sci Instrum* 2006;77:103707.
- [44] Griswold C, Cross WM, Kjerengtroen L, Kellar JJ. Interphase variation in silane-treated glass-fiber-reinforced epoxy composites. *J Adhes Sci Technol* 2005;19(3–5):279–90.
- [45] Hodzic A, Stachurski ZH, Kim JK. Nano-indentation of polymer–glass interfaces. Part I. Experimental and mechanical analysis. *Polymer* 2000;41:6895–905.
- [46] Kim JK, Sham ML, Wu J. Nanoscale characterization of interphase in silane treated glass fibre composites. *Compos Part A: Appl Sci Manuf* 2001;32:607–18.
- [47] Clair B, Arinero R, Lévesque G, Ramonda M, Thibaut B. Imaging the mechanical properties of wood cell wall layers by atomic force modulation microscopy. *IAWA* 2003;24(3):223–30.
- [48] Abe H, Ohtani J, Fukazawa K. FE-SEM observations on the microfibrillar orientation in the secondary wall of tracheids. *IAWA* 1991;12:431–8.
- [49] Xing C, Wang S, Pharr GM, Groom LH. Effect of thermo-mechanical refining pressure on the properties of wood fiber cell walls: measured by nanoindentation and atomic force microscopy. *Holzforschung* 2008;62(2):230–6.
- [50] Jakes JE, Frihart CR, Beecher JF, Moon RJ, Stone DS. Experimental method to account for structural compliance in nanoindentation measurements. *J Mater Res* 2008;23:1113–27.